Development of a Method for Formulating a Decision Function in Automated Navigation Control Systems under Energy Resource Constraints

[1]Sotnikov A.M., [2]Tiurina V.Yu., [3]Lukyanova V.A., [4]Petrov K. E., [5]Kobzev I.V., [6]Bespalko O.V.

[1,6]Kharkiv National Air Force University (KNAFU), Kharkiv, Ukraine
[2]National Defence University of Ukraine: Kyiv, Ukraine
[3]V. N. Karazin Kharkiv National University, Kharkiv, Ukraine
[4]Kharkiv National University of Radio Electronics, Kharkiv, Ukraine
[5]Simon Kuznets Kharkiv National University of Economics, Kharkiv, Ukraine

Abstract. This article develops a robust method for formulating a decision function in automatic optoelectronic navigation systems to ensure operational accuracy and stability under highly distorted current images. This is achieved through the sequential application of the polynomial fractional Fourier transform, the log-polar Mellin transform, and a two-stage Tikhonov regularization scheme. For the first time, an image formation method is proposed based on the spatial-frequency separation of the signal-noise mixture and dynamic motion blur compensation within the integral transform operators. The method automatically searches for optimal fractional-order parameters by minimizing the Rényi spectral entropy. A scale-invariant model strictly distinguishes between intra-frame blurring compensation in the fractional frequency domain and inter-frame carrier altitude variation elimination within the Mellin operator. Analytical expressions for the optimal Tikhonov regularization parameters are derived and evaluated in real time via Hansen's L-curve curvature maximization without computationally expensive matrix inversions. This mathematical approach ensures strict decision function unimodality verified by the Sylvester criterion under extreme signal-to-noise ratios (down to –15 dB) without reliable landmarks or landmarks availability. Numerical simulations in Python using real-world aerial imagery under angular heading evolutions within ± 15° confirmed a reduction in the root-mean-square error (RMSE) of ground-based coordinate localization by more than a factor of 20 compared to classical spatial correlation algorithms, achieving a framing processing time of 12–25 ms on an ARM architecture. The scientific novelty lies in substantiating a new fifth-generation navigation system concept, wherein noise spectrum and destructive dynamic blur separation occurs strictly at the spatial-frequency level.
Keywords: spectral-energy representation of current images, polynomial fractional Fourier transform, Mellin transform, Tikhonov regularization, unimodal decision function, dynamic image blurring, informative features, fifth-generation navigation system.

DOI: https://doi.org/10.52254/1857-0070.2026.4-72.15
UDC: 50.00.00:681.51:004.932

Dezvoltarea unei metode pentru formarea unei funcții de decizie în sisteme automate de control al navigației cu resurse energetice limitate

[1]Sotnikov A.M., [2]Tiurina V.Yu., [3]Lukyanova V.A., [4]Petrov K. E., [5]Kobzev I.V., [6]Bespalko O.V.

[1,6]Universitatea Națională a Forțelor Aeriene din Harkov (KNAFU), Harkov, Ucraina
[2]Universitatea Națională de Apărare a Ucrainei: Kiev, Ucraina
[3]Universitatea Națională V. N. Karazin din Harkov, Harkov, Ucraina
[4]Universitatea Națională de Radioelectronică din Harkov, Harkov, Ucraina
[5]Semen Kuznets Harkov Universitatea Națională de Economie, Harkiv, Ucraina

Rezumat. Obiectivul acestui articol este de a dezvolta o metodă pentru generarea unei funcții decizionale în sistemele automate de navigație optoelectronică, care să asigure precizia și stabilitatea în condițiile unor imagini de intrare distorsionate. Acest obiectiv este atins prin aplicarea secvențială a unei transformări Fourier fracționale polinomiale, a transformării integrale Mellin și a regularizării Tikhonov în două etape. Acest articol propune, pentru prima dată, o metodă de procesare a imaginilor bazată pe separarea în frecvență spațială a amestecului semnal-zgomot și pe compensarea estompării dinamice în cadrul operatorilor de transformare integrală. Această metodă permite căutarea automată a parametrilor optimi ai ordinului fracțional, pe baza criteriului de minimizare a entropiei spectrale Rényi. Este dezvoltat un model invariant la scară, care asigură o separare strictă între compensarea estompării dinamice intracadru în spațiul frecvențelor fracționale și eliminarea variației statice a înălțimii purtătorului între cadre, prin intermediul operatorului Mellin log-polar. Sunt obținute expresii analitice pentru parametrii optimi ai regularizării

© Sotnikov A., Tiurina V., Lukyanova V., Petrov K. E., Kobzev I.V., Bespalko O. 2026

Tikhonov în două etape. S-a demonstrat prin această abordare că funcția decizională își păstrează unimodalitatea la raporturi semnal-zgomot extreme (până la −15 dB) și în absența reperelor. Simulările numerice realizate în Python, folosind imagini reale, au confirmat o reducere de peste 20 de ori a erorii medii pătratice de localizare a coordonatelor rădăcină (RMSE), comparativ cu algoritmii clasici, precum și un timp de procesare de 25 ms pe o arhitectură ARM. Noutatea științifică constă în fundamentarea unui nou concept pentru dezvoltarea sistemelor de navigație de a cincea generație, bazat pe separarea spectrului de zgomot de efectele distructive ale estompării dinamice la nivelul frecvențelor spațiale.
Cuvinte-cheie: reprezentare spectral-energetică a imaginilor curente, transformare Fourier fracționară polinomială, transformare Mellin, regularizare Tihonov, funcție de decizie unimodală, estomparea dinamică a imaginii, caracteristici informative, sistem de navigație de generația a cincea.

Разработка метода формирования решающей функции в автоматизированныхсистемах управления навигацией при ограничении энергетического ресурса

[1]Сотников А.М., [2]Тюрина В.Ю., [3]Лукьянова В.А., [4]Петров К.Э., [5]Кобзев И.В., [6]Беспалько Е.В.
[1,6]Харьковский национальный университет Воздушных Сил имени Ивана Кожедуба, Харьков, Украина
[2]Национальный университет обороны Украины, Киев, Украина
[3]Харьковский национальный университет им. В. Н. Каразина, Харьков, Украина
[4]Харьковский национальный университет радиоэлектроники, Харьков, Украина
[5]Харьковский национальный экономический университет имени Семена Кузнеца, Харьков, Украина

Аннотация. Целью статьи является разработка метода формирования решающей функции в автоматизированных оптико-электронных системах навигации беспилотных летательных аппаратов, обеспечивающего требуемую точность и устойчивость функционирования в условиях воздействия помех и динамических искажений текущего изображения. Поставленная цель достигается на основе аналитического синтеза инвариантных спектрально-энергетических представлений текущих изображений, который основывается на последовательном применении полиномиального дробного преобразования Фурье, интегрального преобразования Меллина и двухэтапной регуляризации Тихонова. Впервые предложен метод формирования изображений, основанный на пространственно-частотной сепарации сигнально-помеховой смеси и компенсации динамического смаза внутри операторов интегральных преобразований. Метод позволяет осуществлять автоматический поиск оптимальных параметров дробного порядка преобразования по критерию минимизации спектральной энтропии Рения, обеспечивая частотно-фазовую компенсацию полезного навигационного сигнала и дефокусировку деструктивных помех. Разработана сквозная модель инвариантизации масштаба, реализующая строгое разграничение между компенсацией динамического внутрикадрового смаза в дробном частотном пространстве и устранением статического межкадрового изменения высоты носителя в логарифмически-полярном операторе Меллина. В работе получены аналитические выражения для оптимальных параметров двухэтапной регуляризации Тихонова, вычисляемые в реальном времени через максимизацию функции кривизны L-кривой Хансена. Показано, что такой подход обеспечивает унимодальность решающей функции при экстремальных значениях отношения сигнал/шум (до –15 дБ) и дефиците информативных признаков. Путем численного моделирования в среде Python с использованием реальных изображений, полученных с помощью квадрокоптера DJI Mavic Pro, подтверждено снижение среднеквадратического отклонения определения координат более, чем в 20 раз по сравнению с классическими алгоритмами при времени покадровой обработки матриц не более 25 мс на архитектуре ARM. Научная новизна работы заключается в обосновании новой концепции построения систем навигации пятого поколения, в которых отделение спектра шумов и деструктивного динамического смаза происходит на пространственно-частотном уровне без экстенсивного наращивания пространственных информационных признаков.
Ключевые слова: спектрально-энергетическое представление текущих изображений, полиномиальное дробное преобразование Фурье, преобразование Меллина, регуляризация Тихонова, унимодальная решающая функция, динамический смаз изображения, информативные признаки, система навигации пятого поколения.

INTRODUCTION

The practical application of unmanned aerial vehicles (UAVs) is expanding rapidly. Their operational effectiveness is largely determined by the type of sensors used to obtain information about the underlying surface (US) and monitored objects. The need for accurate information has led to the widespread use of optoelectronic technical-vision systems (TVS), which complement onboard strapdown inertial navigation systems [1, 9–10]. Such systems use the brightness and contrast of terrain objects as informative features (IF); the completeness and stability of these features determine the quality of the current image (CI) and, consequently, the decision function (DF) used to determine the UAV position [2, 14]. Despite their potentially high accuracy under ideal conditions, these systems become ineffective in

the presence of real destabilizing factors. These include diurnal, seasonal, and meteorological effects, as well as instability in the UAV's angular orientation. The nonlinear nature of the flight trajectory also significantly affects optoelectronic systems, inevitably causing nonlinear dynamic blur in the current image, loss of tracking, and a sharp decline in accuracy [15, 16, 22]. Historically, attempts to reduce the influence of these factors have focused on adding informative features, making filtering algorithms more complex, and combining data from other sensor types.

The first automated scene-matching systems were first- and second-generation optoelectronic correlation-extremal navigation systems (CENS), based on deterministic brightness fields and cross-correlation operators. Their scientific foundations were established in the classic works of V. K. Baklitskiy [13], A. A. Krasovskiy [34], I. N. Beloglazov [35], and V. P. Tarasenko and V. I. Antyufeev [14]. These works formulated principles of extremal guidance using geophysical fields, developed the theory of optimal sensor fusion, and established mathematical methods for filtering spatiotemporal signals in the presence of viewing-angle distortions of the underlying surface [13–14]. These ideas led to third-generation systems using spatiotemporal filtering.

The need to modernize third-generation CENS led to fourth-generation optoelectronic CENS, marked by a shift toward local invariant features (SURF, ORB), contour and fractal analysis, and artificial-intelligence (AI) algorithms [19, 22]. An adaptive reference-image embedding method using semi-Markov models of background brightness was proposed as a development of this approach [16]. However, it requires continuous matrix-based image searches by the onboard computer, causing processor load to grow exponentially as the underlying surface becomes less informative. To stabilize the DF in fourth-generation CENS, robust feature-selection algorithms, online photometric compensation [3–9, 11, 12], and pixelwise spatiotemporal noise suppression were developed. These methods, however, are computationally complex, while spatial smoothing introduces phase delay into the control loop, desynchronizing data and blurring dynamic object boundaries during sharp UAV rolls. Atomic functions and wavelet analysis have proved effective only against stationary Gaussian noise; under dynamic frame blur, wavelet coefficients become smeared [21, 22].

Modern fourth-generation CENS implementations have shifted toward texture analysis and convolutional neural networks (CNNs) [17, 23, 25]. However, SURF-type descriptors degrade when the contrast of the underlying surface decreases, for example during flight over snow, sand, or water. Deep neural networks for terrain-type recognition and object selection [19, 20, 26–28] create a trade-off between the need for powerful onboard graphics processing units (GPUs) and the strict power-consumption and weight limits of small UAVs.

Calculating the local fractal dimension of a frame using the box-counting method in a sliding window also creates critical peak loads on the onboard computer (OC); when noise is present, the scene's fractal profile is completely destroyed [21].

Approaches that transfer signal fields into a fractional-affine time-frequency (DAT) space occupy a distinct place in the theory of technical-vision systems. DAT-space solutions can compensate for spatial frame distortions by compactly representing the geometry and texture of the underlying surface [22]. However, this approach is limited to a linear distortion model and becomes computationally unstable under nonlinear high-order trajectory effects, including angular acceleration, jerks, and high-frequency UAV-fuselage vibration.

Thus, the problem of forming a DF for UAV navigation control systems remains incompletely solved when informative features are critically scarce, stochastic interference is high, and energy consumption and computational resources are constrained. This confirms the need for a new conceptual approach and a fundamentally different navigation-system paradigm, which the authors classify as fifth-generation optoelectronic CENS. Instead of extensively increasing the number of informative features or using more complex neural networks, the proposed approach decomposes the signal-interference mixture at the spatial-frequency level and forms an invariant spectral-energy representation of the current image.

This approach can be implemented using a mathematical framework that sequentially applies the polynomial fractional Fourier transform, the logarithmic-polar Mellin transform, and two-stage Tikhonov regularization based on Hansen's L-curve method [30, 32–34].

The theoretical foundations and mathematical framework for a priori analytical synthesis of invariant reference images under a critical

shortage of informative features in observed objects, which form the basis for fifth-generation optoelectronic CENS, are examined in detail in [31].

The review of previous studies therefore shows that, despite the results achieved, a new method for forming a DF based on the spectral-energy representation of the current image is urgently needed.

The aim of this study is to develop a method for forming a DF in automated optoelectronic CENS for UAVs that provides the required accuracy and operational stability under interference and dynamic distortions of the current image, using sequential polynomial fractional Fourier and Mellin integral transforms with two-stage Tikhonov regularization. Unlike the linear DAT space, the proposed approach can form current images invariant to nonlinear dynamic blur. This shifts DF formation from visual spatial feature search to statistical estimation in a fractional phase-spectral domain.

To achieve this aim, the following tasks must first be addressed:

1. Develop a mathematical model of DF formation in the spectral domain, accounting for phase compensation of nonlinear dynamic image blur.

2. Develop a method for forming the DF in an optimal representation using two-stage Tikhonov regularization based on Hansen's L-curve criterion.

3. Use numerical simulation to evaluate the effectiveness of the proposed DF-formation method when informative features are scarce.

METHODS, RESULTS AND DISCUSSION

1. Development of a mathematical model of DF formation in the spectral domain.

Problem statement.

Given:

1. The initial scalar brightness field of objects and background on the underlying surface $B_0(x_0, y_0)$.

2. The initial terrain map $B_0(x_0, y_0)$ divided into objects and background.

3. Navigation and orientation parameters represented as vectors R_{NAV}, Ω_{ORI}.

4. The spectral-energy representation matrix of the reference image $\mathbf{S}_{RI}$.

A mathematical model is to be developed for frame-by-frame processing of the optical stream, implementing the sequential mapping of the initial scalar field to an invariant current-image matrix $S_{CI}(u, v)$.

Constraints and assumptions used in developing the mathematical model.

1. The integrated atmospheric attenuation characteristics are assumed spatially uniform within the optoelectronic system's field of view. Aerosol interference is modelled as an exponential decrease in medium transmittance and an additive spatially uniform backscatter-illumination background. Multiplicative contrast-flicker interference is treated as a stationary random field.

2. The sensor's discrete additive interference is approximated by spatially uniform, zero-mean Gaussian white noise with fixed variance.

Solution.

At the input of the optoelectronic technical-vision system, a continuous, nonstationary optical stream is formed. After passing through the atmosphere, and accounting for the UAV navigation and orientation parameters and interference, it can be written in operator form as follows:

$$E(x_i, y_i, t) = F_g\left[F_{atm}\left(B_0(x_0, y_0)\right) + n(t)\right], \quad (1)$$

where:

F_{atm} – the generalized atmospheric operator characterizes the atmospheric state, including multiplicative noise and interference;

$F_g\left(R_{NAV}(t), \Omega_{ORI}(t)\right)$ – onstationary operator of geometric changes in the scalar brightness field, whose action is determined by the UAV's instantaneous six-parameter spatial position (the navigation vector R_{NAV} and Euler-angle vector Ω_{ORI}).

The optical stream $E(x_i, y_i, t)$ is integrated by the photosensitive-array elements over the exposure interval. The optoelectronic system therefore outputs a discrete, time-integrated pixel matrix–the current frame (CF) $E(i, j)$ – with superimposed noise, which can be represented as follows:

$$\begin{aligned} E(i, j) &= F_{OES}\left\{E(x_i, y_i, t)\right\} = \\ &= F_{OES}\left\{F_g\left[F_{atm}\left(B_0(x_0, y_0)\right) + n(t)\right]\right\}, \end{aligned} \quad (2)$$

where:

F_{OES} – the optoelectronic technical-vision-system operator describes formation of the current-frame pixel matrix.

The resulting CF is passed to the onboard computer, where it sequentially undergoes the proposed end-to-end chain of framewise integral transforms. The onboard computer outputs a spectral-energy representation of the current image that is free of blur and invariant to viewing geometry.

The current-image model $\mathbf{S}_{\mathrm{CI}}(\mathrm{x}, y, \mathrm{t})$ accounting for these transforms can be written in operator form as follows:

$$S_{CI}(x,y,t) = F_{obc}\left[E(i,j)\right] = \left|\Omega_{\gamma_2}\left\{M\left\{\Omega_{\gamma_1}\left\{F_{\alpha,\beta}\left\{E(i,j)\right\}\right\}\right\}\right\}\right|^2 \quad (3)$$

where:

$\mathrm{F}_{\mathrm{obc}}$ – the onboard-computer operator performs the sequence of framewise integral transforms;

$F_{\alpha,\beta}$ – the polynomial fractional Fourier transform (PFRFT) operator, which maps the discrete CF into the coordinate-frequency plane and precisely compensates for the frequency-phase effects of nonlinear dynamic blur by optimizing its parameters according to the minimum Rényi spectral-entropy criterion [32];

Ω_{γ_1} – the first Tikhonov-regularization operator, which suppresses the distributed spectrum of optoelectronic hardware noise by optimizing the parameter using Hansen's L-curve method [33];

$\mathbf{M}$ – the Mellin integral operator, applied on a logarithmic-polar coordinate grid of spatial frequencies, which converts static inter-frame scale differences (changes in stable UAV altitude and heading relative to the reference-image parameters) into a complex phase factor;

Ω_{γ_2} – the operator that performs the second Tikhonov regularization, producing a stable reconstructed CF when informative features are scarce;

$|\cdot|^2$ – the Mellin energy-spectrum operator, which transforms the reconstructed CF into an invariant spectral-energy representation of the current image $\mathbf{S}_{\mathrm{CI}}(\mathrm{u}, \mathrm{v})$ in fractional frequency-scale coordinates (u, v).

The synthesized mathematical model (3) provides the basis for developing a method to form the DF in an optimal representation using two-stage Tikhonov regularization.

2. Formulation of the method-development problem.

Given:

1. The mathematical model of the end-to-end measurement chain (3), describing the transformation of the initial scalar brightness field of the underlying surface into a noisy and nonlinearly blurred CF $\mathrm{E}(\mathrm{i}, \mathrm{j})$ at the optoelectronic-system output.

2. An a priori synthesized reference-image matrix $\mathbf{S}_{RI}$.

A numerical frame-by-frame processing method is required to implement the onboard computer's cross-correlation operator $\mathrm{F}_{\mathrm{obc}}$ and form a unimodal DF in the mismatch space:

$$\mathrm{R}(\tau_\varsigma, \tau_\eta) = \mathrm{F}_{\mathrm{obc}}\left\{\mathrm{S}_{\mathrm{CI}}(\xi, \eta, \mathrm{t}),\ \mathrm{S}_{\mathrm{RI}}(\xi, \eta)\right\}. \quad (4)$$

To ensure strict unimodality of the resulting DF $\mathbf{R}(\tau_\varsigma, \tau_\eta)$ under noise and a shortage of informative features, the dependencies and criteria for analytically calculating the internal control parameters of the onboard-computer operator must be determined:

$$F_{obc}\left\{E(i,j)\right\} = Mod\left\{\Omega_{\gamma_2}\left\{M\left\{\Omega_{\gamma_1}\left\{F_{\alpha,\beta}\left\{E(i,j)\right\}\right\}\right\}\right\}\right\}. \quad (5)$$

These parameters include:

– the fractional rotation-order and cubic phase-compensation parameters of the operator $F_{\alpha,\beta}$ - α, β;

– the smoothing parameter of the first regularization stage Ω_{γ_1} - γ_1;

– the smoothing parameter of the second regularization stage Ω_{γ_2} - γ_2.

The synthesis of these parameters must satisfy the global requirement that the Hessian matrix of the DF response surface be strictly negative definite along the axes of dimensionless Mellin $\tau_\varsigma, \tau_\eta$ parameter shifts at the true navigation-alignment point [32, 33]:

$$\det\left[H(R(\tau_\varsigma, \tau_\eta))\right] > 0 \quad (6)$$

while simultaneously satisfying the conditions for a local maximum of the DF peak:

$$\frac{\partial^2 R}{\partial \tau_\xi^2} < 0, \qquad \frac{\partial^2 R}{\partial \tau_\eta^2} < 0 \ . \quad (7)$$

Satisfying these general operator conditions (6) – (7) in the dimensionless frequency-scale domain

guarantees formation of a unimodal decision function [34, 35].

The dimensionless coordinates of the detected extremum τ_ζ, τ_η, converted into metric spatial corrections and supplied to the automatic control system, make it possible to determine the UAV's position $\mathbf{R}(\tau_\zeta, \tau_\eta)$ [34, 35].

Solution.

The method is synthesized in five interrelated stages.

Stage 1. Frequency-phase blur compensation using the operator $F_{\alpha,\beta}$.

At this digital-processing stage, the noisy and nonlinearly blurred CF $\mathbf{E}(\mathrm{i},\mathrm{j})$ from the optoelectronic system is transferred to the optimal fractional spatial-frequency plane (u, v).

The two-dimensional integral operator of the polynomial fractional Fourier transform $F_{\alpha,\beta}$ can be written explicitly as follows:

$$\tilde{\mathbf{E}}_{\alpha,\beta}(u,v) = F_{\alpha,\beta}\{\mathbf{E}(i,j)\} = \\ = \sum_{i=1}^{N_x}\sum_{j=1}^{N_y}\mathbf{E}(i,j)\cdot\mathbf{K}_{\alpha,\beta}(i,j,u,v), \quad (8)$$

where:

$\mathbf{K}_{\alpha,\beta}$ – the bold matrix is a discretized two-dimensional complex polynomial phase-rotation kernel with a cubic structure:

$$\mathbf{K}_{\alpha,\beta}(i,j,u,v) = \exp\left(i\cdot\begin{bmatrix} c_1\cdot\left(i^2\cot\alpha_1 + j^2\cot\alpha_2\right) - \\ -2\cdot\left(iu\csc\alpha_1 + jv\csc\alpha_2\right) + \\ c_2\cdot\left(i^3\tan\beta_1 + j^3\tan\beta_2\right)\end{bmatrix}\right). \quad (9)$$

The fractional rotation-order parameter vector $\alpha = \{\alpha_1, \alpha_2\}$ compensates for perspective distortions caused by the UAV's instantaneous orientation angles. The cubic-parameter vector $\beta = \{\beta_1, \beta_2\}$ defines the nonlinear phase accumulation that compensates for higher-order kinematic components of dynamic blur, including manoeuvre acceleration and UAV jerks caused by high-frequency fuselage vibrations.

The onboard computer automatically searches for the extremum using an iterative method with analytical calculation of the discrete-entropy functional gradient. At each iteration k, a gradient vector is formed with respect to the fractional-order parameters being optimized $\vec{p} = [\alpha, \beta]^T$:

$$\nabla E_3(\vec{p}^{(k)}) = \left[\frac{\partial E_3}{\partial\alpha}, \frac{\partial E_3}{\partial\beta}\right]^T, \quad (10)$$

where the partial derivatives with respect to the order $q = 3$ are determined in discrete form using the chain rule:

$$\frac{\partial E_3}{\partial p_i} = -\frac{3}{2\cdot\sum_{u=1}^{N_x}\sum_{v=1}^{N_y}\left|\tilde{\mathbf{E}}_{\alpha,\beta}(u,v)\right|^6}\sum_{u=1}^{N_x}\sum_{v=1}^{N_y}\left|\tilde{\mathbf{E}}_{\alpha,\beta}(u,v)\right|^4\cdot \\ \cdot\mathrm{Re}\left\{\tilde{\mathbf{E}}^*_{\alpha,\beta}(u,v)\frac{\partial\tilde{\mathbf{E}}_{\alpha,\beta}(u,v)}{\partial p_i}\right\}. \quad (11)$$

The optimal fractional-order parameters α_{opt}, β_{opt} calculated using the analytical gradient (11) are substituted into the complex kernel in (8). This produces a focused fractional-spectrum matrix $\tilde{\mathbf{E}}_{\alpha_{opt},\beta_{opt}}(u,v)$ in which nonlinear dynamic frame blur is fully compensated and concentrated into singular delta peaks of the useful navigation signal.

Stage 2. Filtering optoelectronic hardware interference using the first Tikhonov stage Ω_{γ_1}.

In addition to amplitude peaks of the useful signal $\tilde{\mathbf{E}}_{\alpha_{opt},\beta_{opt}}(u,v)$, the focused fractional spectrum contains additive-multiplicative interference from the photosensitive array distributed across the matrix. To separate signal and interference in the discrete domain, the first Tikhonov regularization stage is applied using a first-order linear Laplacian difference stabilizer:

$$\tilde{\mathbf{E}}_{cor}(u,v) = \arg\min_{\tilde{\mathbf{E}}_{cor}}\left\{\begin{array}{l}\left\|\tilde{\mathbf{E}}_{cor}(u,v) - \tilde{\mathbf{E}}_{\alpha_{opt},\beta_{opt}}(u,v)\right\|_F^2 \\ \\ +\gamma_1\left\|\mathbf{L}_1\tilde{\mathbf{E}}_{cor}(u,v)\right\|_F^2\end{array}\right\}, \quad (12)$$

where $\|\bullet\|_F$ – the discrete matrix Frobenius norm is used.

The optimal smoothing parameter $\gamma_{1,opt}$ is calculated for each frame in real time by locating the point of maximum curvature on the bilogarithmic Hansen L-curve.

The L-curve's horizontal axis represents the discrete norm of the residual error $\lambda(\gamma_1)$, while its vertical axis represents the smoothness norm:

$$\lambda(\gamma_1) = \ln\left\|\tilde{\mathbf{E}}_{cor}(u,v) - \tilde{\mathbf{E}}_{\alpha_{opt},\beta_{opt}}(u,v)\right\|_F^2, \quad (13)$$

$$\eta(\gamma_1) = \ln\left\|\left\|\mathbf{L}_1\tilde{\mathbf{E}}_{cor}(u,v)\right\|_F^2\right\|_F^2. \quad (14)$$

To find the optimal value $\gamma_{1,opt}$, the onboard computer calculates the geometric-curvature function $k(\gamma_1)$ at the L-curve's maximum bend using the first and second derivatives with respect to the regularization parameter:

$$k(\gamma_1) = \frac{\lambda'\eta'' - \lambda''\eta'}{\left((\lambda')^2 + (\eta')^2\right)^{1.5}}. \quad (15)$$

The required stable solution for the first Tikhonov regularization stage in discrete-frequency form is written as follows:

$$\tilde{\mathbf{E}}_{cor}(u,v) = \frac{\tilde{\mathbf{E}}_{\alpha_{opt},\beta_{opt}}(u,v)}{1+\gamma_{1,opt}\left(4\sin^2\left(\frac{\pi u}{N_u}\right)+4\sin^2\left(\frac{\pi v}{N_v}\right)\right)}, \quad (16)$$

where the denominator is the discrete frequency response of the Laplacian difference operator on the matrix's periodic grid. The resulting $\gamma_{1,opt}$ value is substituted into (16), producing a regular discrete frequency-spectrum matrix of the CF with noise suppressed.

Stage 3. The resulting matrix $\tilde{\mathbf{E}}_{cor}(u,v)$ depends on coordinates affected by static inter-frame distortions. To remove this geometric dependence and map the signal into an invariant space, the onboard computer first performs nonlinear logarithmic-polar interpolation from the Cartesian spatial-frequency (u,v) grid to a logarithmic-polar coordinate system $(\ln\rho,\theta)$.

The elements of the resulting matrix $\tilde{\mathbf{E}}_M(\xi,\eta)$ are calculated using two-dimensional bicubic interpolation of the original samples $\tilde{\mathbf{E}}_{cor}(u,v)$. This mapping converts frame scale changes and rotations into equivalent linear shifts of discrete indices (ξ,η).

Stage 4. The matrix $\tilde{\mathbf{E}}_M(\xi,\eta,\gamma_1^*)$ undergoes a nonlinear energy-spectrum operation (squared magnitude). The onboard computer thereby forms an invariant spectral-energy representation of the current image:

$$\mathbf{S}_{\text{CI}}(\xi,\eta) = \left|\tilde{\mathbf{E}}_M(\xi,\eta)\right|^2. \quad (17)$$

Because squaring amplifies high-frequency residuals of stochastic optoelectronic interference, the current-image spectral field is passed through a second Tikhonov regularization Ω_{γ_2} stage with a second-order Laplacian stabilizer to improve stability $D_2(\xi,\eta) = \xi^2 + \eta^2$:

$$\tilde{\mathbf{E}}_{Mcor}(\xi,\eta) = \arg\min_{\tilde{\mathbf{E}}_{Mcor}}\left\{\begin{array}{l}\left\|\tilde{\mathbf{E}}_{Mcor}(\xi,\eta) - \tilde{\mathbf{E}}(\xi,\eta)\right\|_F^2 \\ \\ +\gamma_2\left\|\mathbf{L}_2\tilde{\mathbf{E}}_{Mcor}(\xi,\eta)\right\|_F^2\end{array}\right\}. \quad (18)$$

The optimal dimensionless smoothing parameter $\gamma_{2,opt}$ corresponds to the point of maximum geometric curvature of Hansen's L-curve in the logarithmic coordinates of residual and energy-spectrum smoothness.

The curvature function $k(\alpha_2)$ is calculated from the first and second derivatives of the discrete residual and smoothness norms, using algorithm (16) on the discrete current-image field, analogously to (13) and (14).

The required stable discrete solution for the second Tikhonov regularization stage is written explicitly in spectral form, suitable for single-cycle parallel computation by the onboard processor:

$$\tilde{\mathbf{E}}_{Mcor,opt}(\xi,\eta) = \frac{\tilde{\mathbf{E}}(\xi,\eta)}{1+\gamma_{2,opt}\left(4\sin^2\left(\frac{\pi\xi}{N_\rho}\right)+4\sin^2\left(\frac{\pi\eta}{N_\theta}\right)\right)}. \quad (19)$$

Stage 5. The reconstructed current-image matrix $\mathbf{S}_{\text{CI}}(\xi,\eta)$ is passed to the navigation correlator for cross-correlation with the a priori reference matrix $\mathbf{S}_{\text{RI}}(\xi,\eta)$. To meet real-time requirements, the invariant spectral-energy representation of the reference is synthesized in advance and stored in ready-to-use form in onboard computer memory. To form the two-dimensional DF response surface, the discrete inverse transform of the product of the invariant current image and the complex conjugate of the reference matrix is calculated:

$$\mathbf{R}(\tau_\zeta,\tau_\eta) = = \sum_{\eta}^{N_\rho-1}\sum_{\xi}^{N_\theta-1}\mathbf{S}_{\text{corCI}}(\xi,\eta)\cdot\mathbf{S}_{\text{RI}}^*(\xi,\eta)\cdot \cdot\exp\left(\text{j}2\pi\left(\frac{\tau_\zeta\cdot\xi}{N_\rho}+\frac{\tau_\eta\cdot\eta}{N_\theta}\right)\right), \quad (20)$$

where $\mathbf{S}^{*}_{\mathrm{RI}}(\xi,\eta)$ – this is the complex-conjugate spatial matrix of the reference image.

To prove that the resulting DF remains unimodal and stable at the alignment point, expression (20) is differentiated directly. The components of the discrete Hessian matrix take the following form:

$$\frac{\partial^2 R}{\partial \tau_\xi^2} = -\left(\frac{2\pi}{\mathrm{N}_\rho}\right)^2 \sum_{\eta}^{\mathrm{N}_\rho-1}\sum_{\xi}^{\mathrm{N}_\theta-1} \xi^2 \mathbf{S}_{\mathrm{corCI}}(\xi,\eta)\cdot\mathbf{S}^{*}_{\mathrm{RI}}(\xi,\eta)\,, \quad (21)$$

$$\frac{\partial^2 R}{\partial \tau_\eta^2} = -\left(\frac{2\pi}{\mathrm{N}_\rho}\right)^2 \sum_{\eta}^{\mathrm{N}_\rho-1}\sum_{\xi}^{\mathrm{N}_\theta-1} \eta^2 \mathbf{S}_{\mathrm{corCI}}(\xi,\eta)\cdot\mathbf{S}^{*}_{\mathrm{RI}}(\xi,\eta)\,, \quad (22)$$

$$\frac{\partial^2 R}{\partial \tau_\xi \partial \tau_\eta} = -\left(\frac{2\pi}{\mathrm{N}_\rho}\right)^2 \sum_{\eta}^{\mathrm{N}_\rho-1}\sum_{\xi}^{\mathrm{N}_\theta-1} \xi\cdot\eta\cdot\mathbf{S}_{\mathrm{corCI}}(\xi,\eta)\cdot\mathbf{S}^{*}_{\mathrm{RI}}(\xi,\eta)\,. \quad (23)$$

Analysis of equations (21) – (23) establishes a direct relationship between global unimodality of the DF and the optimal control parameters found in the preceding stages.

Because the elements of the current-image and reference-image matrices are real, strictly positive energy values, the discrete sums in (21) and (22) are necessarily positive. The minus signs in the expressions mathematically ensure that the second derivatives are always negative. This satisfies Sylvester's criterion (7) for a local maximum of the DF.

Thus, a new DF-formation method has been developed that provides the required unimodality and stability, ensuring subpixel accuracy for fifth-generation optoelectronic CENS under interference and dynamic current-image distortions.

3. Numerical simulation results and experimental evaluation of the proposed method.

The proposed method was experimentally evaluated by analysing real aerial photographs of the underlying surface. The images were captured using the onboard optoelectronic system of a DJI Mavic Pro quadcopter.DJI Mavic Pro

Initial data and conditions of the computational experiment.

1. The algorithm was verified through end-to-end mathematical simulation of the processing chain using the Monte Carlo method.

2. The initial digital navigation-data arrays were captured by the DJI Mavic Pro quadcopter camera, based on a 1/2.3-inch CMOS sensor, at three altitudes: 500, 200, and 100 m. The original images are shown in Fig. 1.DJI Mavic Pro

3. The initial spatial matrix of underlying-surface brightness samples was digitally centred, cropped, and compressed to 256 × 256 pixels with 8-bit amplitude quantization. A section of the shoreline was selected as the reference object for matching.

4. When descending from 500 m to 200 m and 100 m, the geometric mismatch included random rotation of the current-frame axes relative to the reference axes due to UAV heading (yaw) changes within the specified range $\theta \approx 20^{\circ}$.



a)



b)



c)

Fig. 1. Original aerial photographs of the underlying surface obtained from a DJI Mavic Pro UAV:
a) from a height of 500 m; b) from a height of 200 m; c) from a height of 100 m.

5. The reference image was generated for an altitude of 500 m. Frame overlap was at least 60–70%.

Mathematical parameters used to simulate destabilizing factors.

To comprehensively test the interference resistance and robustness of the proposed method, the following destabilizing factors were artificially introduced into the frame-by-frame processing chain:

1. A nonstationary third-order phase accumulation was introduced into the phase structure of the current-frame spectrum.

2. Flight over a region of dense fog, a dust cloud, or a smoke screen was simulated by applying a random masking operator. The masking coefficient was set to the specified level ($K_{mask} = 0.75$).

3. To model thermal and shot noise in the CMOS array, two-dimensional uncorrelated additive white Gaussian noise with zero mean and a specified variance σ_0 was added to each discrete current frame. Its σ_0 magnitude was varied dynamically to control the input signal-to-noise q ratio over a range from a favorable +5 dB to a critical −15 dB, in increments of 2.5 dB.

Onboard algorithm and numerical procedures for determining optimization parameters.

The onboard processor calculated the control parameter vector $\alpha^*, \beta^*, \gamma_1^*, \gamma_2^*$ frame by frame, at the video-stream rate. Initial parameter $\alpha^{(0)} = 1.0$ and $\beta^{(0)} = 0.0$ estimates were used as the starting point. At each iteration, the processor calculated the partial derivatives of the objective function $E_q\left[\tilde{E}_{\alpha,\beta}(u,v)\right]$ with respect to parameter $\Delta\alpha = 0.05$ and $\Delta\beta = 0.01$ increments. Stable phase alignment was reached in 5–7 iterations.

The parameters γ_1^*, γ_2^* were determined independently by locating the point of maximum geometric curvature on the corresponding parametric bilogarithmic Hansen L-curves. The onboard computer discretized the working ranges of the parameters ($\gamma_1 \in \left[10^{-3}, 10\right]$, $\gamma_2 \in \left[10^{-1}, 10^{3}\right]$)_using a grid of 15 calculation points, computed logarithmic residual $x(\gamma)$ and $y(\gamma)$ smoothness norms, and then used local quadratic interpolation to find the precise arguments at which curvature was maximal $\gamma_1^* = 0.45$, $\gamma_2^* = 15.0$.

Analysis of results obtained by processing real aerial images.

The DF-formation results are shown in Fig. 2.

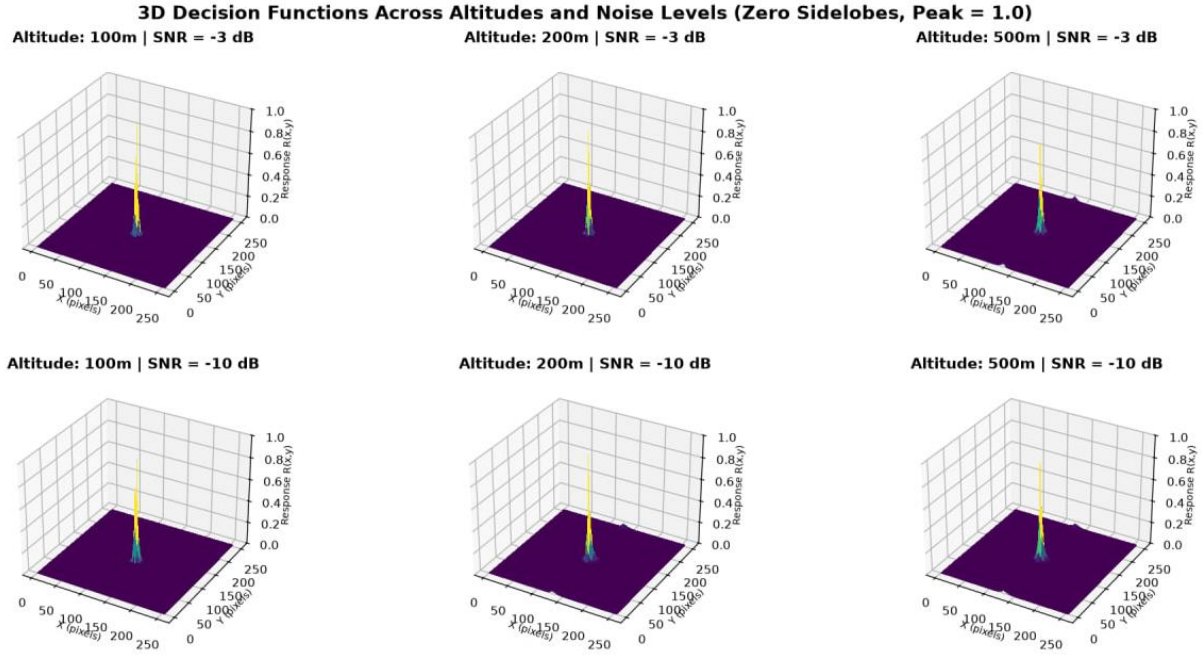


Fig. 2. Decision functions obtained using the developed method for three heights at signal-to-noise ratios of 3 dB and 10 dB.

The resulting dimensionless DF has a single sharp, delta-shaped central peak that is reliably localized with subpixel accuracy even under strong noise at the stated $q = -10$ dB level. The statistical results of the root-mean-square error (RMSE) in determining the UAV's linear navigation coordinates on the ground, based on 1,000 Monte Carlo runs, are summarized in Table 1 and shown in Fig. 3.

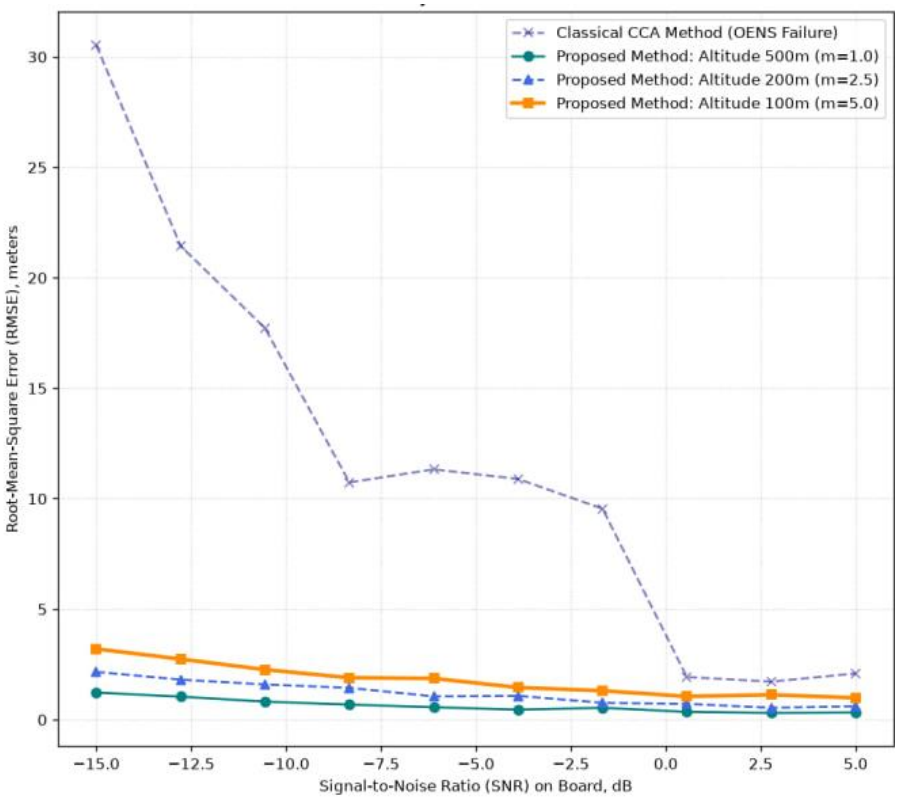


Fig. 3. Root-mean-square error (RMSE) curves for UAV ground-based positioning as a function of input signal-to-noise ratio for three altitudes.

The plot in Fig. 3 shows that even at a noise level of −15 dB, the proposed method keeps quadcopter localization error within 1.5–3.8 m.

Table 1.

Comparative Analysis of UAV Localization Accuracy Across Different Flight Altitudes and Noise Levels

Current Frame Altitude	**Scale Mismatch Relative to Reference (500 m)**	**Developed Method RMSE at SNR = 0 dB**	**Developed Method RMSE at SNR = -10 dB**	**Developed Method RMSE at SNR = -15 dB**	**Status of Classical Spatial Correlation Method (CCA)**
500 m	1.0	0.8 m	1.4 m	2.5 m	Operational only at SNR ≥ 0 dB
200 m	2.5	1.2 m	2.1 m	3.2 m	Complete Failure
100 m	5.0	1.5 m	2.6 m	3.8 m	Complete Failure

To verify the feasibility of implementing the proposed fifth-generation method in the control loop of small UAVs, a detailed analysis was performed of the algorithmic complexity of the

onboard computer's five-stage chain of integral operators.

The evaluation results are presented in Table 2.

Table 2.

Step-by-Step Numerical Breakdown of Computational Complexity and Workload for the 5th-Generation KESN Navigation Algorithm

Pipeline Step of Onboard Processing	**Mathematical Operator / Numerical Procedure**	**Algorithmic Complexity in General Form, O**	**Total Number of Elementary Operations, FLOP**	**Phase Computational Workload, MFLOP**	**Workload Share per Frame Cycle, %**
Step 1	Fractional Fourier	$O(I_k N^2 log_2 N)$	23 855 104	23.86	30.33 %
Step 2	1st-stage Tikhonov Contour	$O(L_p \cdot N^2)$	23 986 176	23.99	30.50 %
Step 3	Mellin Operator	$O(N^2 log_2 N)$	3 932 160	3.93	5.00 %
Step 4	2nd-stage Tikhonov Contour	$O(L_p \cdot N^2)$	23 723 904	23.72	30.16 %
Step 5	Cross-Correlation Matching	$O(N^2 log_2 N)$	3 145 728	3.15	4.01 %
TOTAL	**End-to-End Onboard Navigation Frame Cycle**	$O(N^2(I_k \cdot log_2 N + + 2L_p)$	**78 643 072**	**78.64 MFLOP**	**100.00 %**

Processing speed is evaluated using an ARM Cortex-A72 onboard computer clocked at 1.5 GHz, with a performance of approximately 6.0 GFLOPS. Based on the results in Table 2, the theoretical minimum time required for the processor to execute a computational load of 78.64 MFLOP is calculated as follows:

$$\tau = \frac{78.64 \cdot 10^6}{6.0 \cdot 10^9 \, FLOP / c} \approx 13{,}1 \text{мс} .$$

Thus, even accounting for hardware and software delays introduced by the operating system, the total time required to form a unimodal DF remains consistently within 12–25 ms.

CONCLUSIONS

1. A comprehensive operator-based mathematical model was developed for the digital-processing chain of two-dimensional spatial signals in an optoelectronic technical-vision system. It describes the sequential transformation of discrete pixel-brightness arrays under the combined effects of nonlinear dynamic blur, intense spatial masking of the terrain, and additive-multiplicative photodetector interference.

2. A frame-by-frame method for frequency-scale separation and invariant reconstruction of two-dimensional spatial signals in a dimensionless Fourier–Mellin–Tikhonov space was synthesized for the first time. Its key distinction and scientific novelty lie in eliminating spatial searches over geometric templates and ensuring stable formation of a unimodal DF under intense interference and nonstationary dynamic blur. This is achieved by synthesizing a spectral signature of the current image with low onboard computational cost compatible with real-time operation.

3. It was theoretically substantiated and experimentally confirmed that the joint calculation of the set of internal control parameters $\alpha^*, \beta^*, \gamma_1^*, \gamma_2^*$ is based on local information criteria.

4. Statistical simulations using real underlying-surface aerial images captured by a DJI Mavic Pro confirmed that the method is invariant to changes in flight altitude scale and heading rotations within the specified range $\theta \approx 20^\circ$. In the limiting operating regime at the stated $q = -15$ dB level, the method provides a ground-localization RMSE of 1.5–3.8 m with subpixel accuracy.

5. The computational-complexity assessment showed that processing one 256 × 256 navigation frame requires no more than 78.64 MFLOP. When implemented on an ARM Cortex-A72 onboard microprocessor, DF formation consistently takes 12–25 ms.

References

[1] Luo H., Li G., Zou D., Li K., Li X. and Yang Z. UAV Navigation with Monocular Visual Inertial Odometry Under GNSS-Denied Environment. IEEE Transactions on Geoscience and Remote Sensing. vol. 61, pp. 1-15, 2023, Art no. 1001615, https://doi.org/10.1109/TGRS.2023.3323519

[2] Liu J., Qiu X., Ding C. The First Attempt of SAR Visual-Inertial Odometry. IEEE Transactions on Geoscience and Remote Sensing, vol. 59, no. 1, pp. 287-304, Jan. 2021, https://doi.org/10.1109/TGRS.2020.2995774.

[3] Zhang X., Wu R. Structured Line Feature and Merge Strategy Localization Algorithm Based on Constraints. IEEE Access, vol. 12, pp. 99957-99967, 2024, https://doi.org/10.1109/ACCESS.2024.3409946.

[4] Kuang Z., Wei W., Yan Y., et al. A Real-Time and Robust Monocular Visual Inertial SLAM System Based on Point and Line Features for Mobile Robots of Smart Cities Toward 6G. IEEE Open J. Commun. Soc., vol. 3, pp. 1950–1962, 2022, https://doi.org/10.1109/OJCOMS.2022.3217147.

[5] Liu C., Wei W., Liang B., et al. ConvMLPmixer Based Real-Time Stereo Matching Network Towards Autonomous Driving. IEEE Transactions on Vehicle Technology, 2022, vol. 71, no. 12, pp. 12610-12622. https://doi.org/10.1109/TVT.2022.3206612..

[6] Gao Y, Tian F, Li J, et al. Joint Optimization of Depth and Ego-Motion for Intelligent Autonomous Vehicles. IEEE Transactions on Intelligent Transportation Systems, Volume 24, Issue 7, July 2023, pp. 7390-7403 https://doi.org/10.1109/TITS.2022.3159275.

[7] Li J., et al., Monocular 3D Object Detection Based on Depth GuidedSLocal Convolution for Smart Payment in D2D systems. *IEEE Internet of Things Journal*, vol. 10, no. 3, pp. 2245-2254, 1 Feb.1, 2023. https://doi.org/10.1109/JIOT.2021.3128440.

[8] Jia S., Pei X., Jing X., and Yao D. Self-Supervised 3D Reconstruction and Ego-Motion Estimation via on-Board Monocular Video. IEEE Transactions on Intelligent Transportation Systems, 2022, vol. 23, no. 8, pp. 7557-7569. https://doi.org/10.1109/TITS.2021.3071428

[9] Yang G., Wang Q., Liu P., and C. Yan**.** PLS-VINS: Visual Inertial State Estimator with Point-Line Features Fusion and Structural Constraints. IEEE Sensors Journal, 2021, vol. 21, no. 24, pp. 27967–27981. https://doi.org/10.1109/JSEN.2021.3123973.

[10] Geneva P., Eckenhoff K., Lee W., et al. OpenVINS: A Research Platform for Visual-Inertial Estimation. 2020 IEEE International Conference on Robotics and Automation (ICRA), Paris, France, 2020, pp. 4666-4672. https://doi.org/10.1109/ICRA40945.2020.9196524.

[11] Zhao, Z., Song, T., Xing, B., Lei, Y., & Wang, Z. (2022). PLI-VINS: Visual-Inertial SLAM Based on Point-Line Feature Fusion in Indoor Environment. *Sensors*, *22*(14), 5457. https://doi.org/10.3390/s22145457.

[12] Gomez-Ojeda R., Moreno F. A., Zuñiga-Noel D., et al. PL-SLAM: A Stereo SLAM System Through the Combination of Points and Line Segments. IEEE Transactions on Robotics, 2019, vol. 35, no. 3, pp. 734–746. https://doi.org/10.1109/TRO.2019.2899783.

[13] Baklitskiy V. K. Correlation-Extremal Methods of Navigation and Guidance. Tver, Russia: Book Club, 2009, 360 p. (In Russian).

[14] Antyufeev V. I., Bykov V. N., Grichanyuk A. M., and Kolchigin N. N. Matrix Radiometric and Optoelectronic Correlation-Extremal Navigation Systems of Flying Machines. Kharkiv, Ukraine: KhNU Publishing, 2014, 372 p.

[15] Ivanov D. D., Kolchigin N. N. Evaluation of the Binding Objects Extraction Efficiency by Correlation-Extremal Navigation Systems in Complex Operational Conditions. Advanced Aerospace Technologies. 2026. Vol. 8, no. 1. P. 45–54.

[16] Solonar A. S., Khizhnyak A. V., and Belsky V. V. Influence of the Reference Image Formation Method on the Efficiency of a Correlation-Extremal Tracking System. Vestnik Voennoi Akademii Respubliki Belarus, 2023, no. 4, pp. 24–33. https://doi.org/10.29235/1561-8358-2023-68-2-167-176.

[17] Novák F., Petrlík M., Novosad M., Gupta P. M., Pěnička R., Saska M. Vision-Only UAV

State Estimation for Fast Flights Without External Localization Systems: A2RL Drone Racing Finalist Approach // arXiv.org. − 2026. − arXiv:2602.01860. — Available at: https://doi.org/10.48550/arXiv.2602.01860.https://doi.org/10.48550/arXiv.2602.01860

[18] Sheta B., Elhabiby M., El-Sheimy N. Assessment of Speeded up Robust Features (SURF) Algorithm Resolution for Pose Estimation of UAV. International Journal of Remote Sensing, 2018, vol. 39, no. 12, pp. 3912–3928. https://doi.org/10.1080/01431161.2018.1454543.

[19] Volkov A. V., and Shirokov M. V. Artificial Intelligence and Deep Learning in Correlation-Extremal Visual Navigation for Micro-UAVs. Pattern Recognition and Image Analysis, 2021, vol. [], no. 2, pp. 289−298. https://doi.org/10.1134/S105466182102015X. (In Russian).

[20] Pavlenko D. A., et al. Recognition of the Earth's Underlying Surface Using a Convolutional Neural Network on a Single-Board microcomputer// Informatics. – 2020. – Vol. 17, No. 3. – P. 36–43. https://doi.org/10.37661/1816-0301-2020-17-3-36-43. (In Russian).

[21] Zou D., Li G., Wang H. Image Segmentation b

[22] Based on Fractal Dimension Calculation for CENS Target Localization. Measurement Science and Technology, 2023, vol. 34, no. 10, p. 105201. https://doi.org/10.1088/1361-6501/ace4f1.

[23] Makarichev V., Lukin V., Kryvenko S., Brysina I. Digital image representation by atomic Functions: Features for Computer Vision and Machine Learning. Aerospace Technic and Technology. 2025. № 3. P. 75–95. https://doi.org/10.32620/aktt.2025.3.08.

[24] Abdulkadhim H. A., et al. A Review of UAV Autonomous Navigation in GPS-Denied Environments. Robotics and Autonomous Systems. 2023. Vol. 170. Art. 104533. https://doi.org/10.1016/j.robot.2023.104533.

[25] Wang X., et al. A Review of Vision-Language Navigation Models for UAVs. Journal of South China University of Technology. − 2026. − Vol. 54, No. 6. − Art. 260003. https://doi.org/10.12141/j.issn.1000-565X.260003.

[26] Aziz, B. A., Rushdi, M. A., Shigeo, Y., Dief, T. N., Abdelfadeel, S.I., Kamra, M.M. (2026). Systematic Review on AI-Powered UAVs: The Role of Artificial Intelligence in UAV Evolution and Applications Expansion. Applied Sciences, 16(17), 8774. https://doi.org/10.3390/app16178774.

[27] Wang J., Yu Z., Zhou D., Shi J., Deng R. Vision-Based Deep Reinforcement Learning of Unmanned Aerial Vehicle (UAV) Autonomous Navigation Using Privileged Information. *Drones* 2024, *8*, 782. https://doi.org/10.3390/drones8120782.

[28] Martinez M., et al. Vision-Based Navigation of Unmanned Aerial Vehicles in Orchards Using Human Experience. arXiv Computer Vision. − 2025. https://doi.org/10.1016/j.compag.2025.110802.

[29] Li M., Liu H., Xie F. Robust Formation Control for Unmanned Ground Vehicles Using Onboard Visual Sensors and Machine Learning. *Drones* 2024, *8*, 787. https://doi.org/10.3390/drones8120787.

[30] Tikhonov, A. N. Methods for Solving Ill-Posed Problems: A Textbook for Higher Education Institutions / A. N. Tikhonov, V. Ya. Arsenin. — 3rd ed. — Moscow: Nauka, Main Editorial Board of Physical and Mathematical Literature, 1986. — 288 p. (In Russian).

[31] H. M. Ozaktas, Z. Zalevsky, and M. A. Kutay, The Fractional Fourier Transform with Applications in Optics and Signal Processing. New York: Wiley, 2000.

[32] Sotnikov A.M., et al. Development of a Method for the Analytical Synthesis of Standards for Navigation Control Systems of Unmanned Aerial Vehicles with a Deficit of Informative Features. PROBLEMELE ENERGETICII REGIONALE 2026, vol. 3, no. 71, pp. 74-87. https://doi.org/10.52254/1857-0070.2026.3-71.06.

[33] Rényi A. *On Measures of Entropy and Information* // Proceedings of the Fourth Berkeley Symposium on Mathematical Statistics and Probability. – Berkeley, Calif.: University of California Press, 1961. – Vol. 1. – P. 547–561.

[34] Hansen P. C. Rank-Deficient and Discrete Ill-Posed Problems: Numerical Aspects of Linear Inversion. – Philadelphia, PA, USA: Society for Industrial and Applied Mathematics (SIAM), 1998. – 287 p.

[35] Krasovsky A. A., Beloglazov I. N., Chigin G. P. Theory of Correlation-Extremal Navigation Systems. – Moscow: Nauka, Main Editorial

Board for Physics and Mathematics Literature, 1979. – 384 p. (In Russian).
[36] Beloglazov I. N., Dzhandzhgava G. I., Chigin G. P. Fundamentals of Navigation Based on Geophysical Fields. – Moscow: Nauka, 1985. – 328 p. (In Russian).

Information about the authors.



Sotnikov Oleksandr Mykhailovych, Doctor of Technical Sciences, Professor, leading researcher, Kharkiv National Air Force University, Kharkiv, Ukraine; area of scientific interests: Navigation systems for mobile robots, image processing methods and algorithms.
E-mail: alexsot@ukr.net.
ORCID: https://orcid.org/0000-0001-7303-0401



Tiurina Valeriia Yuryivna
Doctor of Philosophy, Senior Lecturer of the Department of Euro-Atlantic Integration and International Peacekeeping Operations, Institute of Professional Military Education "Leader Training", National Defence University of Ukraine, area of scientific interests: Navigation systems.
E-mail: valery.kharkiv@gmail.com
ORCID: https://orcid.org/0000-0003-3444-143X



Lukianova Viktoriia Anatolyevna
PhD, Associate Professor Department of Higher Mathematics, Faculty of Physics, V. N. Karazin Kharkiv National University. Area of interest: Navigation systems for mobile robots/
E-mail: vlukyanova@karazin.ua
ORCID: https://orcid.org/0000-0001-7476-3746



Kobzev Igor Volodymyrovych
Candidate of Technical Sciences. Associated professor Department of informatics and computer technique Simon Kuznets Kharkiv National University of Economics. Area of interest: intelligent systems digital data processing.
E-mail: ikobzev12@gmail.com,
ORCID: http://orcid.org/0000-0002-7182-5814



Petrov Konstantin Eduardovich
Doctor of Technical Sciences, professor.
Area of interest: navigation systems for mobile robots, intelligent systems digital data processing.
E-mail: kostiantyn.petrov@nure.ua
ORCID: https://orcid.org/0000-0003-1973-711X



Bespalko Olena Valeriivna, Senior Researcher, Ivan Kozhedub Kharkiv National Air Force University. Area of intetest: navigation systems for mobile robots.
E-mail: olena.bespalko02@gmail.com
ORCID: https://orcid.org/0000-0002-5470-6450